Regular Article

PHYSICAL CHEMISTRY RESEARCH
Published by the
Iranian Chemical Society
www.physchemres.org
info@physchemres.org

Phys. Chem. Res., Vol. 9, No. 1, 107-121, March 2021
DOI: 10.22036/pcr.2020.246898.1827

Detection of Cyanogen Halides by B_{36} Nanocluster: DFT Study

N. Tayebi[a] and F. Shojaie[b,*]

[a]*Department of Nanotechnology, Graduate University of Advanced Technology, Kerman, Iran*
[b]*Semiconductors group, Institute of Science and High Technology and Environmental Sciences, Graduate University of Advanced Technology, Kerman, Iran*

(Received 6 September 2020, Accepted 15 November 2020)

The adsorption of cyanogen halide gases (CNX) onto the surface of B_{36} nanocluster was investigated using density functional theory (DFT). The results show that the N-head of CNX molecules interacts strongly with the B_{36} nanocluster and adsorption sites on the edge of B_{36} nanocluster are more reactive than those on other sites. The nature of the interaction and binding properties of CNX and B_{36} nanocluster are calculated by molecular orbitals (HOMO and LUMO), topological analysis, global reactivity parameters, density of states, analysis of bond length and bond order. Based on the results, the electrical conductivity of B_{36} nanocluster significantly increases in the presence of CNX molecules. These results suggest that the B_{36} nanocluster could be a promising material in designing CNX sensors.

Keywords: B_{36} nanocluster, Cyanogen halide, Sensor, Topological analysis, Density functional theory

INTRODUCTION

Cyanogen halides CNX (X = F, Cl, Br) are colorless, reactive and volatile gasses with a linear structure [1]. Cyanide gases, used as chemical gases in modern wars, are highly toxic, especially CNCl and CNBr. So that exposure to these gases can cause vomiting, drowsiness, coughing, seizures, headaches, sore throats, swelling and death [2]. It is important to find a quick and easy way to detect these gases in the environment. Detection methods such as spectrophotometry, electrochemistry, and gas chromatography require complex and very expensive devices [3,4]. Hence, finding a simple, inexpensive, fast, reliable sensor helps us to detect cyanogen halides easily. Nanostructured materials have been considered as special materials due to their high surface-to-volume ratio and their unique electrical properties [5,6]. The B_{36} nanocluster is one of these nanostructures. Boron is carbon's neighbor in the periodic table and its valance orbitals are similar to carbon. It cannot have a graphene-like structure with a hexagonal honeycomb framework, due to electron deficiency [7-13]. The synthesis of a quasi-planer born (B_{36} nanocluster) with a hexagonal hole in the center has been reported [13]. It has a perfect hexagonal symmetry (C_{6v}) with a highly stable sheet. Several studies have been performed on the electrical, magnetic, thermodynamic, and optical properties of B_{36} nanocluster [14-16]. Using first-principle calculations, thermal properties of B_{36} nanocluster has been studied [17]. Due to the special properties of B_{36} nanocluster, research has been done on its use in biochemistry [18] and hydrogen storage [19]. The sensing properties of B_{36} nanocluster to detect gas molecules, including CO, N_2, H_2O, O_2, NO and H_2 have been studied by Valadbeigi *et al.* [20]. They demonstrated that B_{36} nanocluster may be employed as a good sensor for detection of CO, O_2 and NO molecules. The adsorption of formaldehyde molecule on B_{36} sheet has been investigated using B97D density functional [21]. The dissociative adsorption of ammonia onto the surface of a B_{36} sheet has been investigated by density functional theory calculations [22]. Theoretical investigation of reactivity and electronic sensitivity of B_{36} toward four nucleobases of adenine,

*Corresponding author. E-mail: f.shojaie@kgut.ac.ir

guanine, thymine, and cytosine has been carried out [18]. The adsorption of HCN on the B_{36} have been studied using B97D level of theory [23]. Also, characteristics of the ring and linear structures of the boron cluster B36 and its doped clusters have been investigated using DFT calculations [24]. In this work, we studied the interaction and adsorption of cyanogen halide molecules, CNX (X = F, Cl, Br), on the neutral B_{36} nanocluster. The results may help us to show B_{36} nanocluster is a good sensor for detection of cyanogen halide gases.

COMPUTATIONAL MODELLING

All geometrical optimizations and quantum chemical calculations of B_{36} cluster and its CNX complexes were performed using Gaussian09 [25].The B97D level [26] of theory with 6-31G+(d) basis set was selected for the calculations. Many research groups have shown the accuracy of B97D for B_{36} borophene [18,21-23]. The use of 6-31G+(d) for B_{36} in theoretical calculations has been observed in several papers [21,22,27].To determine the nature of interaction between cyanogen halides atoms and B_{36} atoms, the topological analysis of the electron densities was performed with the help of a multifunctional wavefunction (Multiwfn) analyzer [28] and the quantum theory of atoms in molecules (QTAIM). The fuzzy bond order (FBO) [29] of B_{36}-CNX complex was calculated by Multiwfn code. In addition, the electron localization function (ELF) [30] was also calculated by Multiwfn code. The atomic charges were calculated by Hirshfeld method using Multiwfn code. The atomic charges provide sufficient information regarding the charge transfer (Q) between the cyanogen halides and B_{36}. In order to predict the most stable structure among six B_{36}-CNX complexes, quantum chemical parameters were investigated. The quantum chemical parameters can be used to obtain information about the chemical reactivity of molecules. The most important of these descriptors are energy gap (E_g), and electronegativity (χ). The energy gap between the HOMO and LUMO levels is an important function of reactivity of a molecule and is calculated using Eq. (1).

$$E_g = E_{LUMO} - E_{HOMO} \quad (1)$$

The electronegativity is calculated by Eq. (2).

$$\chi = -\frac{E_{HOMO} + E_{LUMO}}{2} \quad (2)$$

An index for electronic sensitivity of B_{36} and CNX is the shift of the HOMO-LUMO energy gap and is obtained by Eq. (3),

$$\Delta E_g = \left[\frac{(E_{g2} - E_{g1})}{E_{g1}}\right] \times 100 \quad (3)$$

where E_{g1} and E_{g2} are energy gaps of B_{36} nanocluster and its complexes, respectively.

The adsorption energies resulting from interaction between the CNX molecules and the B_{36} can be obtained from Eq. (4),

$$\Delta E_{ads} = E_{B36-nCNX} - (E_{B36} + nE_{CNX}) \quad (4)$$

where B_{36}-nCNX corresponds to the electronic energy of the B_{36}-CNX complex, E_{B36} is the energy of the isolated borophene, E_{CNX} is the energy of cyanogen halide and n is 1 or 2.

RESULTS AND DISCUSSION

The optimized geometry of B_{36} nanocluster is shown in Fig. 1. The structural surface is not completely planar and has a curvature with a central hexagonal hole. This characteristic of B_{36} surface is in agreement with previous experimental and theoretical studies [13]. Figure 1 shows there are five categories of boron atom that can be recognized in B_{36} structure (1, 2, 3, 4 and 5) plus a central hexagonal hole (6). Six interactions sites of B_{36} cluster with cyanogen halides were studied. The optimized structures of these complexes are shown in Figs. 2, 3 and 4. It should be noted that B_{36} nanocluster can interact with cyanogen halides through F, Cl and Br atoms, but these interactions do not form stable optimized structures. Optimized structures related to the interaction of cyanogen halides (*via* F, Cl and Br atoms) with B_{36} nanocluster on absorption site 1 are shown in Fig. 5. The head of X or N was located near the electrophile sites (B atoms) of the B_{36} cluster for all

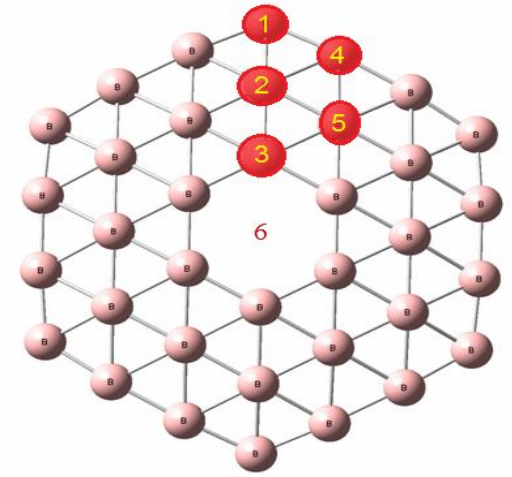

Fig. 1. The structures of optimized geometry of B_{36} cluster.

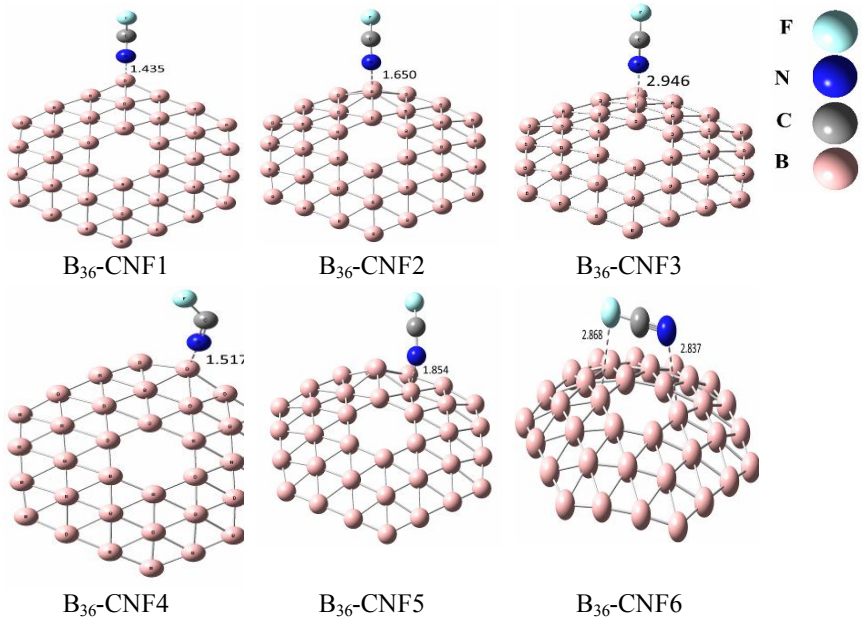

Fig. 2. The most stable structures of B_{36}-CNF complexes. Distances are in Å.

configurations, and then all structures were optimized. The frequency calculations were performed in order to verify and confirm the minima of all obtained stationary points. Therefore, several initial configurations were optimized by placing the N, F, Cl or Br atom of cyanogen halide molecules on different B_{36} boron atoms. The most favorable adsorption configurations show that N atom of CNX attacks to the electron deficient boron atoms of B_{36}. The most stable structures resulting from interactions between CNX and B_{36} are configurations where the N head of CNX axis aligns perpendicular to the B atoms in sites 1, 2, 3, 4 and 5 and is parallel to 6-membered ring of the B_{36} surface. In order

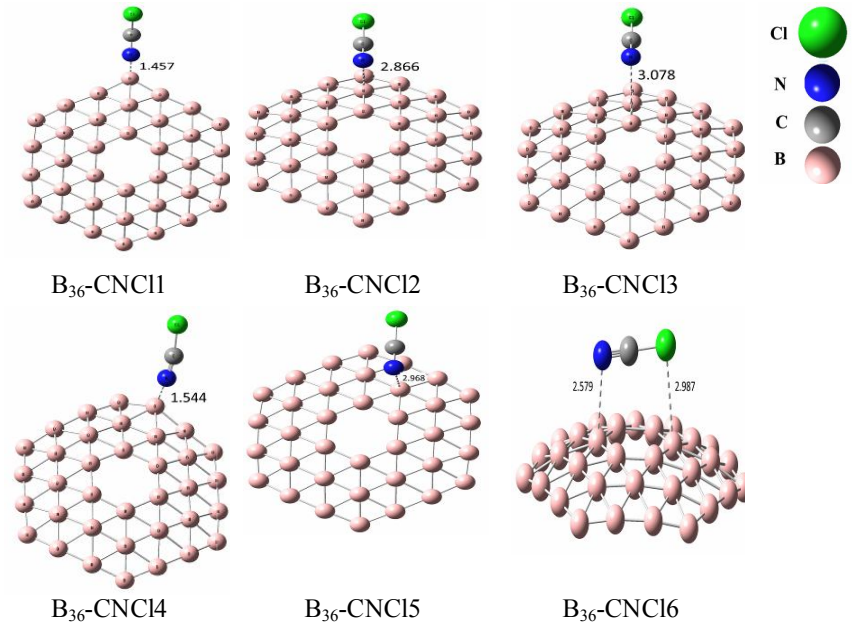

Fig. 3. The most stable structures of B_{36}-CNCl complexes. Distances are in Å.

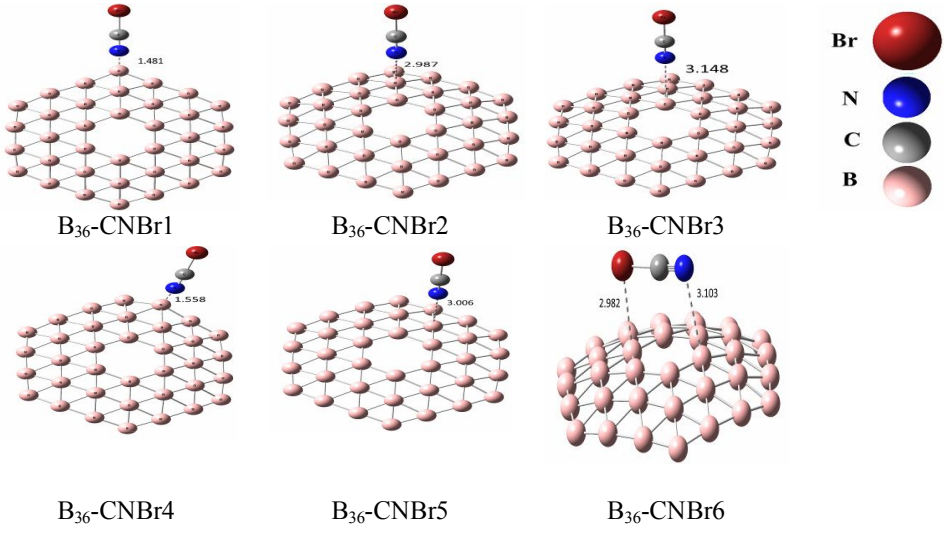

Fig. 4. The most stable structures of B_{36}-CNBr complexes. Distances are in Å.

to study the adsorption characteristics, we name six B_{36}-CNX complexes as B_{36}-NCX1, B_{36}-NCX2, B_{36}-NCX3, B_{36}-NCX4, B_{36}-NCX5 and B_{36}-NCX6 where 1, 2, 3, 4, 5 and 6 refer to adsorption sites on the B atoms of B_{36}.

Adsorption of CNX on B_{36}

Table 1 shows the quantum chemical parameters of CNX, B_{36} nanocluster and six types of B_{36}-CNX complexes. The CNBr molecule in the free state has less energy gap than other two molecules, CNF and CNCl. After adsorption

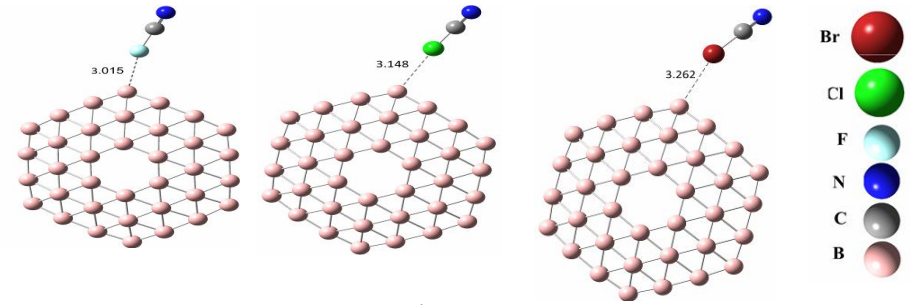

B_{36}-CNF1 B_{36}-CNCl1 B_{36}-CNBr1

Fig. 5. The most stable structures of B_{36}-CNF1, B_{36}-CNCl1 and B_{36}-CNBr1 complexes (*via* F, Cl and Br atoms). Distances are in Å.

Table 1. The Energy Gap, Electronegativity and the Absolute Value of the Change in Energy Gap for the Complexes Being Studied

Complex	E_g (eV)	X (eV)	$\|\Delta E_g\|$ (%)
CNF	6.854	5.692	-
CNCl	5.942	5.500	-
CNBr	5.343	5.391	
B_{36}	1.083	4.788	-
B_{36}-CNF1	0.557	5.005	48.569
B_{36}CNF2	0.816	4.827	24.654
B_{36}-CNF3	1.055	4.581	2.585
B_{36}-CNF4	0.575	4.859	46.907
B_{36}-CNF5	0.981	4.695	9.418
B_{36}-CNF6	1.037	4.731	4.247
B_{36}-CNCl1	0.627	4.739	42.105
B_{36}-CNCl2	1.037	4.612	4.247
B_{36}-CNCl3	1.078	4.786	0.462
B_{36}-CNCl4	0.678	4.647	37.396
B_{36}-CNCl5	1.052	4.579	2.862
B_{36}-CNCl6	1.066	4.596	1.570
B_{36}-CNBr1	0.867	4.435	19.945
B_{36}-CNBr2	1.065	4.824	1.662
B_{36}-CNBr3	1.082	4.752	0.092
B_{36}-CNBr4	0.895	4.265	17.359
B_{36}-CNBr5	1.059	4.715	2.216
B_{36}-CNBr6	1.072	4.695	1.016

Table 2. The Energy Gap and the HOMO and LUMO Energies Obtained in this Study and other Studies

E_{LUMO} (eV)	E_{HOMO} (eV)	E_g (eV)	Method/basis set	Ref.
-3.97	-5.51	1.54	TPSSH/6-311+G(d)	[27]
-4.01	-5.05	1.04	B97D/6-31G(d)	[21]
-4.25	-5.35	1.10	B97D/6-31+G(d)	[21]
-4.30	-5.39	1.09	B97D/6-311+G(d,p)	[21]
-3.85	-5.73	1.88	B3LYP-D3(BJ)/6-311+G(d,p)	[31]
-4.30	-5.39	1.09	B97-D3(BJ)/6-311+G(d,p)	[31]
-4.01	-5.1	1.09	B97D/6-31+G(d)	[18]
-4.247	-5.330	1.083	B97D/6-31+G(d)	This work

via the N-head, energy gap of the B_{36}-CNX complex decreased in comparison to free state CNX. Table 1 indicates that B_{36}-CNX type-1 and type-4 complexes have low energy gap when compared to other B_{36}-CNX complexes. Also, the energy gap of type-1 and type-4 complexes is significantly smaller than B_{36} cluster. This indicates that the reactivity of the complex systems is higher than the reactivity of B_{36} cluster. It can be concluded that B_{36}-CNF complex tends to absorb more electrons than B_{36}-CNCl and also B_{36}-CNCl absorbs more electrons than B_{36}-CNBr, by comparing electronegativity in all types of B_{36} complex systems. Therefore, the interaction of cyanogen halides with B_{36} cluster causes an increase in electronegativity of B_{36}-CNX complex systems, but decreases their energy gap. These changes are more noticeable in B_{36}-CNX type-1 and type-4 complexes. It implies stronger interactions have been performed on absorption sites 1 and 4 of B_{36}-CNX complexes. Table 1 shows $|\Delta Eg|$ values for these configurations vary in the range 0.092% and 48.569%. Table 1 shows the maximum change of ΔE_g is for absorption sites 1 and 4 of B_{36}-CNX complexes. The results show B_{36}-CNBr complex is more stable than B_{36}-CNCl complex and B_{36}-CNCl complex is more stable than B_{36}-CNF complex (especially in type-1 and type-4). Also, the results of the energy gap and energies of HOMO and LUMO for this work and the others' work for B_{36} nanocluster are shown in Table 2. This Table shows that the results of this work are almost the same as the results of the DFT-D methodology. Density of states (DOS) spectra may help to gain a deeper understanding of the effect of interaction between cyanogen gases and B_{36} on sites 1 to 6. In order to study this effect, DOS were calculated and plotted in Fig. 6 (for the two absorption sites 1 and 4), indicating that the trend of DOS spectra is similar to the trend of energy gap. The differences between energy gaps in the two absorption sites 1 and 4 are 0.018, 0.051 and 0.028 eV, and this small difference is also seen in the DOS spectra for B_{36}-CNF, B_{36}-CNCl, B_{36}-CNBr, respectively. Also, the DOS plots indicate that after the CNX adsorption on B_{36}, new states appeared within the E_g that significantly reduce it. Overall, LUMO levels are largely stabilized, and HOMO levels are destabilized slightly, thus E_g is decreased.

The HOMOs of B_{36}-CNF, B_{36}-CNCl and B_{36}-CNBr are in the ranges -5.146 to -5.283 eV, -4.986 to -5.325 eV and -4.712 to -5.356 eV and their LUMOs are in the ranges -4.053 to -4.726 eV, -4.053to -4.425 and -3.817 to -4.291 eV, respectively. The HOMO and LUMO of B_{36}-CNX complexes for sites of 1 and 4 have changed significantly compared with HOMO and LUMO of B_{36}. These results show that B_{36}-CNX type-1 and type-4

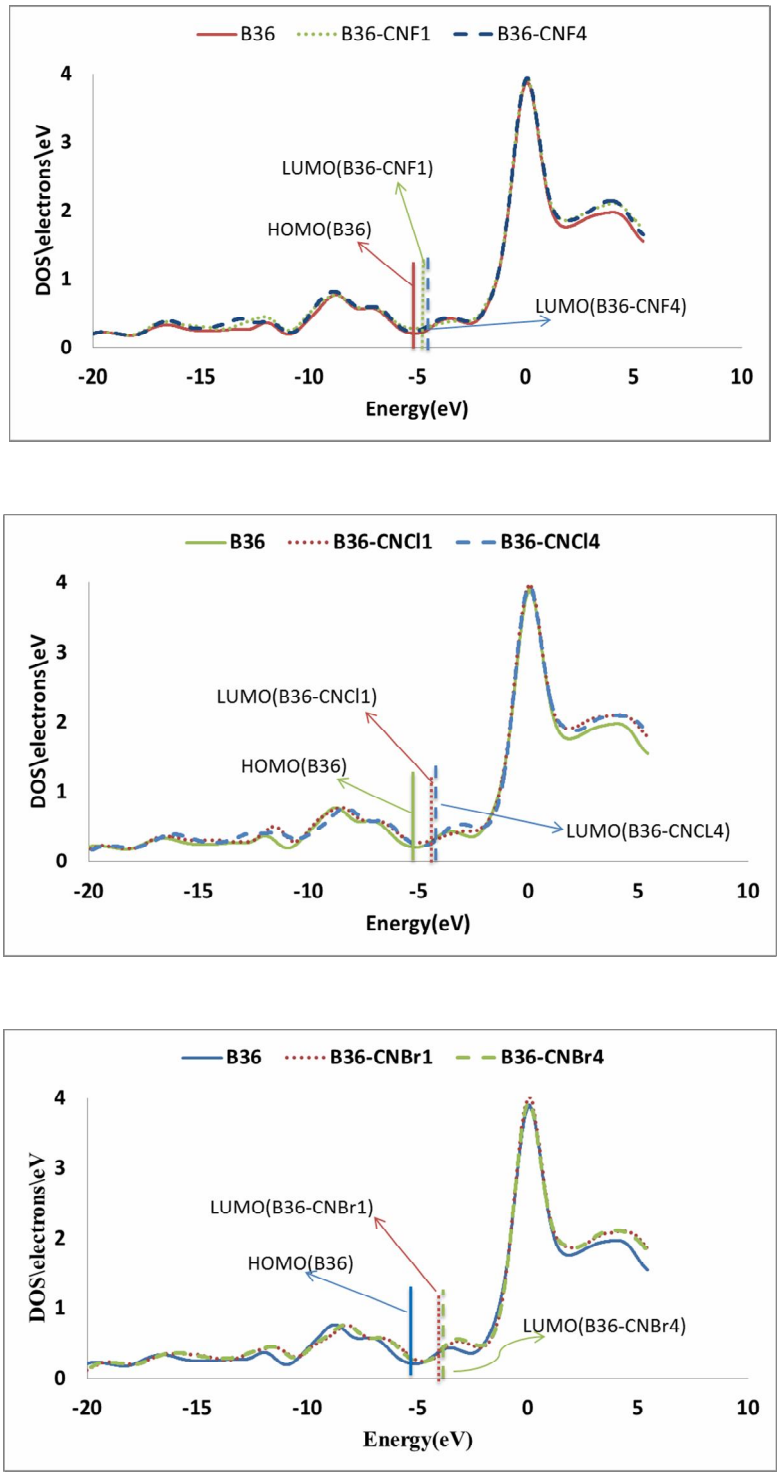

Fig. 6. DOS of the optimized B_{36}-CNX1 and B36-CNX4 geometries.

complexes have been formed as a result of stronger interactions than other types. The boron atoms at the edge of B_{36} are more reactive and these results are in agreement with theoretical studies reported in references [18,20,21,27,31].

In order to characterize the B_{36}-CNX bonds, bond lengths and bond orders were calculated. The lengths and orders of the bonds are shown in Table 3 for the two absorption sites 1 and 4. Table 3 shows that an increase in the B-B bond length complex is similar to that in B_{36} nanocluster B-B bond length, and as a result the bond order decreases. Differences between the bond lengths of B_{36}-CNX complexes are insignificant. The bond orders of C-N bonds are 2.822, 2.787 and 2.780 for CNF, CNCl and CNBr, respectively, which are close to theirs triple bonds. These bond orders decrease after the interaction between CNX and B_{36} for all absorption sites. The structures of B_{36}-CNX1 and B_{36}-CNX4 are presented in Fig. 7.

Table 4 shows that B_{36}-CNF1 is the most stable complex. The calculated interaction energy is -2.186 eV and the length of the newly formed bond is about 1.435 Å. The second most stable complex is B_{36}-CNF4 with interaction energy of about -1.462 eV. The adsorption energies of B_{36}-CNF3, B_{36}-CNF5 and B_{36}-CNF6 are in the range of -0.500 to -0.578 eV and they are negligible. The most stable complex of B_{36}-CNCl structures is B_{36}-CNCl1 with the interaction energy of about -2.128 eV. The newly adsorption N-B bond is strong and its length is about 1.457 Å. The energy released by complex B_{36}-CNCl4 is about 1.573 eV. It seems B_{36}-CNCl4 is less stable than B_{36}-CNCl1. The B_{36}-CNCl2, B_{36}-CNCl3, B_36-CNCl5 and B_{36}-CNCl6 are the most unstable complexes which are the products of weak interactions. Thus, the inner boron atoms are not favorable adsorption sites in comparison to the edge atoms. The CNBr attaches to the B atom of B_{36} in order to form B_{36}-CNBr. The B_{36}-CNBr1 and B_{36}-CNBr4 configurations correspond to the adsorptions of the CNBr molecule at the B_{36} edge with adsorptions energies of -5.201 and -4.429 eV, respectively. These structures are stable and the most stable complex is B_{36}-CNBr1. Tables 1 and 4 indicate that after the adsorption process, the trend of charge transfer from CNX to B_{36} is in agreement with the trend of electronegativity reduction. The electronegativity of B_36-CNX type-1 complex is more than that of B_{36}-CNX type-4 and charge transfer of B_{36}-CNX type-4 complex is more than that of B_{36}-CNX type-1. As electronegativity of B_{36}-CNF complexes are more than that of B_{36}-CNCl and B_{36}-CNBr, charge transfer of B_{36}-CNBr is increased significantly in comparison with B_{36}-CNCl and B_{36}-CNF. Increasing the atomic number of the halogen in the CNX causes more increase in charge transfer. In addition, the dipole moments play an important role in the charge transfer.

Electrical conductivity is exponentially related to energy gap according to the following relation:

$$\sigma = AT^{3/2} \exp(-E_g/2kT) \quad (5)$$

where k is Boltzmann's constant and A is a constant (electrons/m^3 $K^{3/2}$). It has been shown that this equation is in agreement with the experimental results and calculated change of energy gap. After the adsorption process, B_{36} can generate an electrical signal (used as a portion of an electric circuit) which depends on the amount of energy gap. Based on this equation large, reduction of energy gap will significantly increase the electrical conductance of B_{36}. It means that a gas sensor operates based on the change of its electrical conductivity upon the gas adsorption and charge transfer. Thus, B_{36} can selectively detect the gases of CNX, because of their different effect on the electrical conductivity. Therefore, B_{36} may be a promising gas sensor for detection of CNX gases because of a charge transfer and the reduction of E_g in adsorption process.

In order to study the adsorption effect of CNX molecules on B_{36}, the adsorption of 2CNX molecules on the B_{36} cluster was examined. To this effect, the most stable configuration (site 1) was selected and CNX molecules were added to interaction process. Figure 8 shows the optimized structures of these configurations. Tables 4 and 5 show that the adsorption energy is not significantly affected by the number of CNX molecule. However, the energy gap is more decreased by increasing the number of CNX molecules. Therefore, the electrical conductance of B_{36} is sensitive to the concentration (or pressure) of CNX gas.

The bond critical point (BCP) is a saddle point in the distribution of the electron density ($\rho(r)$), where the electron density gradient ($\nabla\rho(r)$) is zero. The BCP is distinguished by λ_1, λ_2 and λ_3 (three local curvatures),

Table 3. Fuzzy Bond Order (FBO) and Bond Distance (Å) of Complexes B_{36}-CNX. The Numbers in Parentheses are Values for the Free Molecules

Complexes	FBO				Bond length				
	C37-N38	B32-B3	B32-B11	B32-B12	C37-N38	C37-X	B32-B3	B32-B11	B32-B12
B_{36}-CNF1	2.210	0.848	0.848	0.509	1.209	1.336	1.693	1.693	1.784
	(2.822)	(1.115)	(1.115)	(0.716)	(1.184)	(1.324)	(1.597)	(1.597)	(1.649)
B_{36}-CNCl1	2.311	0.866	0.866	0.546	1.189	1.679	1.680	1.680	1.757
	(2.787)	(1.115)	(1.115)	(0.716)	(1.185)	(1.711)	(1.597)	(1.597)	(1.649)
B_{36}-CNBr1	2.317	0.870	0.870	0.571	1.174	1.763	1.669	1.669	1.722
	(2.780)	(1.115)	(1.115)	(0.716)	(1.185)	(1.829)	(1.597)	(1.597)	(1.649)
	C37-N38	B17-B18	B17-B24	B17-B26	C37-N38	C37-X	B17-B18	B17-B24	B17-B26
B_{36}-CNF4	2.292	0.461	0.749	0.431	1.200	1.329	1.833	1.724	1.869
	(2.822)	(0.638)	(0.870)	(0.584)	(1.184)	(1.324)	(1.711)	(1.677)	(1.746)
B_{36}-CNCl4	2.459	0.482	0.747	0.449	1.172	1.633	1.811	1.745	1.847
	(2.787)	(0.638)	(0.870)	(0.584)	(1.185)	(1.711)	(1.711)	(1.677)	(1.746)
B_{36}-CNBr4	2.465	0.487	0.742	0.452	1.170	1.771	1.805	1.745	1.844
	(2.780)	(0.638)	(0.870)	(0.584)	(1.185)	(1.829)	(1.711)	(1.677)	(1.746)

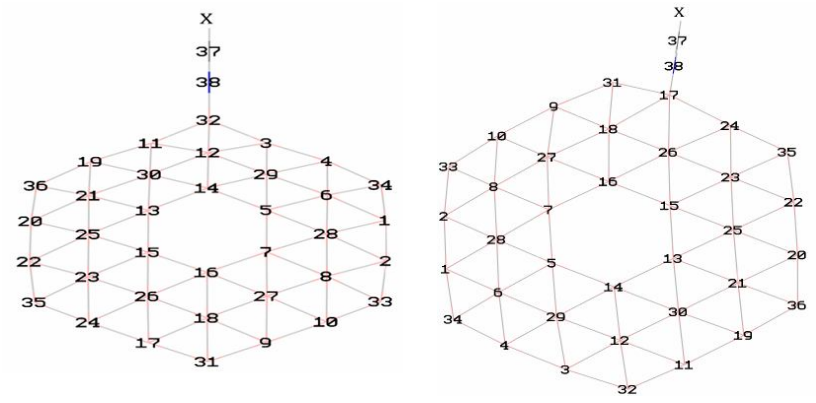

B_{36}-CNX1 B_{36}-CNX4

Fig. 7. The structures of B_{36}-CNX1 and B_{36}-CNX4.

Table 4. Adsorption Energies, C-X Distances, Dipole Moments and Charge Transfers for B_{36}-CNX1 and B_{36}-CNX4

Complex	E_{ad} (eV)	D (Å)	Dipole moment (D)	Q_T (e)
B_{36}-CNF1	-2.186	1.435	2.729	0.003
B_{36}-CNF4	-1.462	1.517	2.867	0.039
B_{36}-CNCl1	-2.128	1.457	6.035	0.158
B_{36}-CNCl4	-1.573	1.544	6.241	0.239
B_{36}-CNBr1	-5.201	1.481	12.635	0.345
B_{36}-CNBr4	-4.429	1.558	12.808	0.353

Table 5. HOMO and LUMO Energies, Energy Gap, Electronegativity and the Absolute Value of the change in Energy Gap, Adsorption Energy and Charge Transfers for B_{36}-2CNX1

Complex	E_{HOMO} (eV)	E_{LUMO} (eV)	E_g (eV)	χ (eV)	$\lvert\Delta Eg\rvert$ (%)	E_{ad} (eV)	Q_T (e)
B_{36}-2CNF1	-5.206	-4.906	0.300	5.056	72.299	-2.153	0.039
B_{36}-2CNCl1	-4.800	-4.392	0.408	4.596	62.327	-2.105	0.299
B_{36}-2CNBr1	-4.243	-3.475	0.768	3.859	29.086	-5.167	0.661

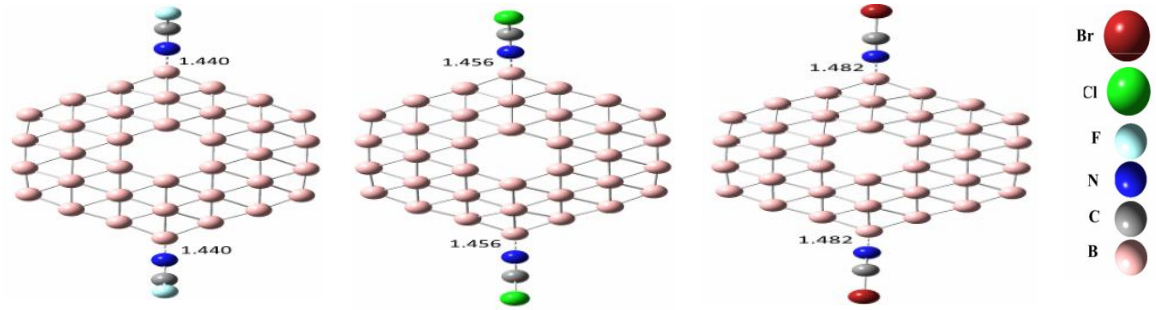

B_{36}-2CNF1 B_{36}-2CNCl1 B_{36}-2CNBr1

Fig. 8. Adsorption of 2 numbers of HCN molecules at the edge of a B_{36} complex. Distances are in Å.

Table 6. Electron Density Descriptors (a.u.) at the Bond Critical Points (BCP) between Atoms of B_{36}-CNX1and B_{36}-CNX4

Complex	BCP	ρ(r)	$\nabla^2\rho(r)$	E(r)	$-\frac{G(r)}{V(r)}$	$\frac{G(r)}{\rho(r)}$
	C37-N38	0.404	0.107	-0.697	5.091	1.789
B_{36}-CNF1	N38-B32	0.171	0.749	-0.118	0.714	1.783
	B32-B3	0.143	-0.272	-0.100	2.458	2.286
	B32-B11	0.139	-0.219	-0.924	2.904	2.697
	C37-N38	0.416	0.365	-0.715	5.302	1.937
B_{36}-CNCl1	N38-B32	0.159	0.725	-0.104	0.733	1.798
	B32-B3	0.145	-0.269	-0.101	2.533	2.358
	B32-B11	0.145	-0.269	-0.101	2.533	2.358
	C37-N38	0.428	0.561	-0.736	4.894	2.049
B_{36}-CNBr1	N38-B32	0.147	0.697	-0.907	0.477	1.802
	B32-B3	0.146	-0.262	-0.102	2.623	2.479
	B32-B11	0.146	-0.262	-0.102	2.623	2.479
	C37-N38	0.411	0.139	-0.712	5.151	1.817
B_{36}-CNF4	N38-B17	0.139	0.533	-0.934	0.706	1.625
	B17-B24	0.134	-0.250	-0.869	2.189	1.699
	B17-B31	0.147	-0.271	-0.104	2.605	2.517
	C37-N38	0.430	0.527	-0.742	5.428	2.030
B_{36}-CNCl4	N38-B17	0.120	0.498	-0.734	0.730	1.650
	B17-B24	0.134	0.240	-0.847	2.247	1.828
	B17-B31	0.147	0.264	-0.102	2.630	2.469
	C37-N38	0.432	0.548	-0.746	5.417	2.043
B_{36}-CNBr4	N38-B17	0.122	0.515	-0.747	0.703	1.663
	B17-B24	0.133	-0.239	-0.845	2.226	1.857
	B17-B31	0.174	-0.261	-0.101	2.637	2.476

which are the main diameter elements of the Hessian matrix of electron density [32]. The electron density distribution is maximum which means λ_1 and λ_2 are negative and perpendicular to the bond path. Also, the electron density is minimum which means λ_3 is positive and tangential to the bond path. The sum of three curvatures or eigenvalues of

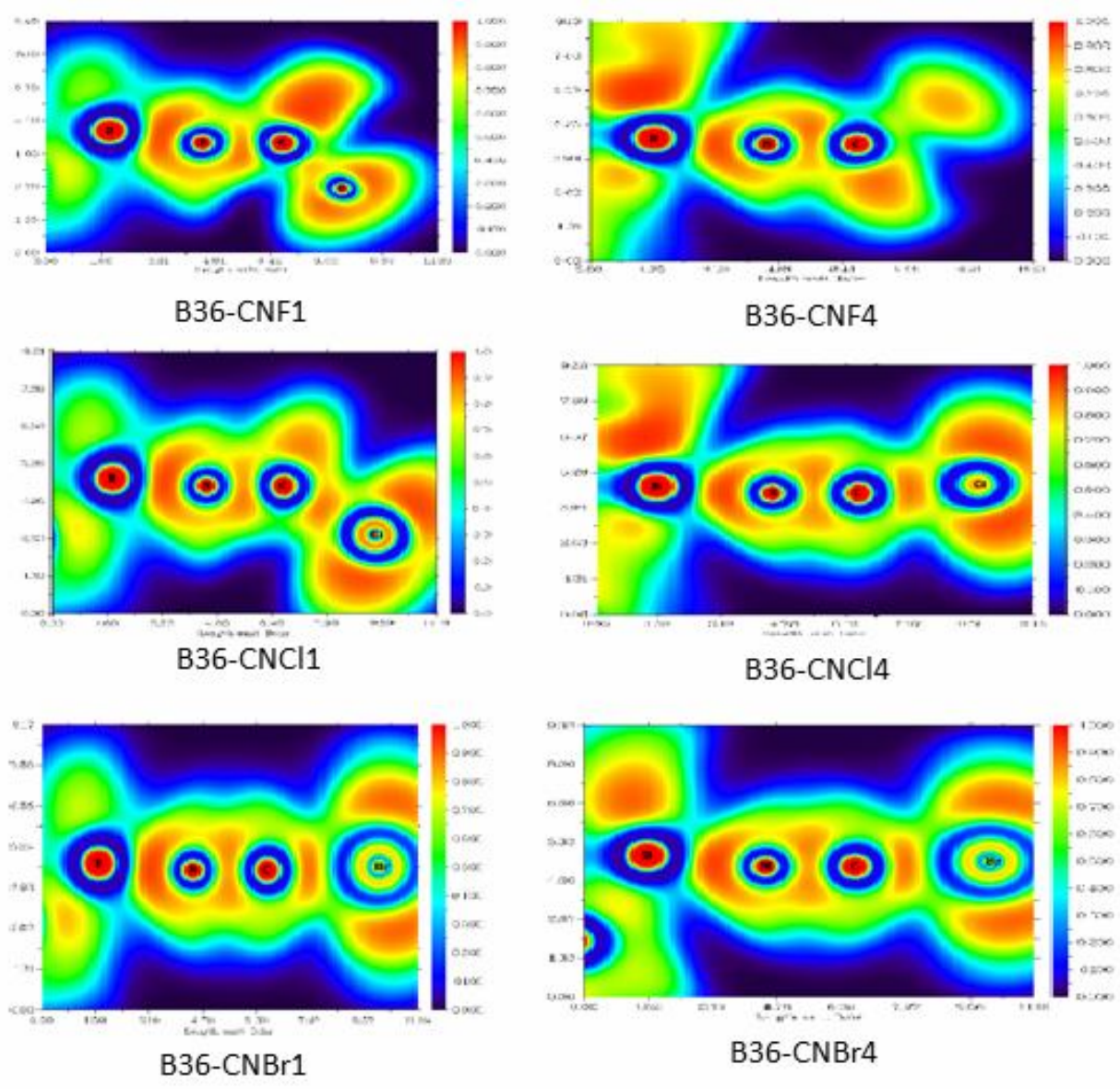

Fig. 9. ELF plots of the optimized B_{36}-CNX complex.

the density at a point is the Laplacian of the electron density at that point ($\nabla^2\rho(r)$). The negative Laplacian is associated with electron concentration, and positive Laplacian shows electron depletion. Equation (6) shows the relationship between the local energy density (E(r)) and the Laplacian of the electron density.

$$E(r) = \frac{1}{4}\nabla^2\rho(r) - G(r) = V(r) + G(r) \quad (6)$$

G(r) is the kinetic energy density, which is always a positive quantity, and V(r) is the potential energy density. These quantities can be evaluated at BCP.

The numerical values of kinetic and potential energy densities at BCP determine the nature of chemical bonds. The interaction is of covalent type if $\nabla^2\rho(r) < 0$, $E(r) < 0$, $\rho(r) > 0.02$, $-\frac{G(r)}{V(r)} < 1$ and $\frac{G(r)}{\rho(r)} < 1$. If $\nabla^2\rho(r) > 0$, $E(r) > 0$,

$\rho(r) < 0.10$, $-\frac{G(r)}{V(r)} > 1$ and $\frac{G(r)}{\rho(r)} > 1$, then the observed interaction is of ionic type [33,34]. Topological analysis of electron density has been performed by researchers to characterize the nature of different chemical bonds. Electron density descriptors at BCP for the key atoms of cyanogen gases and B_{36} nanocluster, and the interaction between cyanogen gases and B_{36} nanocluster are given in Table 6. The topological analyses have been performed for all sites of absorption. Table 6 shows the results of the two absorption sites (1 and 4). Local energy densities are all negative for B_{36}-CNX complexes in sites 1 and 4. The ρ(r) values are bigger than 0.02 for all complexes. Table 6 shows N38-B32 and N38-B17 of B_{36}-CNX type-1 and type-4 complexes. The $\rho(r)$, E(r) and -G(r)/V(r) indicate the nature of the interaction is not purely covalent or ionic. These bonds may be described as covalent-ionic type. All B_{36} nanocluster bonds are covalent-ionic type, but more covalent than ionic.

The electron localization function (ELF) analysis was performed to get further insight into the properties of the bonding interactions. This analysis can provide useful information on chemical bonds of the systems. The ELF value is between zero and one. As ELF increases, the electrons become more localized and concentrated, the ionic nature of the atomic bond between two atoms transform gradually into covalent type. Figure 9 shows ELF images for all compounds. ELF for the bond between interaction cyanogen gases and B_{36} is between 0.5 and 0.55. The ELF analysis reveals those bonds are relatively more covalent, which is in agreement with the electron density analysis.

CONCLUSIONS

Interaction of CNX molecules with the B_{36} nanocluster is investigated by the DFT modelling method. It is found that the CNX molecules interact somewhat strongly with the boron atoms of the B_{36} nanocluster *via* the N-head with appreciable adsorption energy. Also, the adsorption of CNX molecules on the B_{36} nanocluster is studied by six different configurations. In these configurations the edge B atoms of B_{36} nanocluster are more reactive to CNX molecules than the inner atoms. The results suggest that the presence of CNX molecules can be detected by B_{36} nanocluster due to changing the electronic properties. Furthermore, it is found that B_{36} nanocluster is sensitive to the concentration of CNX molecules so that increasing the number of CNX molecules will alter the B_{36} conductance. In addition, adsorption energies show that B_{36}-CNBr complex is more stable than B_{36}-CNCl complex and in turn B_{36}-CNCl complex is more stable than B_{36}-CNF complex.

REFERENCES

[1] Vessally, E.; Behmagham, F.; Massuomi, B.; Hosseinian, A.; Nejati, K., Selective detection of cyanogen halides by BN nanocluster: a DFT study. *J. Mol. Model* **2017**, *23*, 138, DOI: 10.1007/s00894-017-3312-1.

[2] Yang, X.; Shang, C., Quantification of aqueous cyanogen chloride and cyanogen bromide in environmental samples by MIMS. *Water Res.* **2005**, *39*, 1709-1718, DOI: 10.1016/j.watres.2005.01.030.

[3] Thomas, S. W.; Venkatesan, K.; Müller, P.; Swager, T. M., Dark-field oxidative addition-based chemosensing: New bis-cyclometalated Pt(II) complexes and phosphorescent detection of cyanogen halides. *J. Am. Chem. Soc.* **2006**, *128*, 16641-16648, DOI: 10.1021/ja065645z.

[4] Cancho, B.; Ventura, F.; Galceran, M. T., Simultaneous determination of cyanogen chloride and cyanogen bromide in treated water at sub-μg/L levels by a new solid-phase microextraction-gas chromatographic-electron-capture detection method. *J. Chromatogr. A* **2000**, *897*, 307-315, DOI: DOI: 10.1016/S0021-9673(00)00786-X.

[5] Dequesnes, M.; Rotkin, S. V.; Aluru, N. R., Parameterization of continuum theories for single wall carbon nanotube switches by molecular dynamics simulations. *J. Comput. Electron* **2002**, *1*, 313-316, DOI: 10.1023/A:1020722818600.

[6] Bogue, R., Nanosensors: A review of recent progress. *Sens. Rev.* **2008**, *28*, 12-17, DOI: 10.1108/02602280810849965.

[7] Kunstmann, J.; Quandt, A., Broad boron sheets and boron nanotubes: an ab initio study of structural, electronic, and mechanical properties. *Phys. Rev. B* **2006**, *74*, 035413, DOI: 10.1103/

PhysRevB.74.035413.

[8] Tang, H.; Ismail-Beigi, S., Novel precursors for boron nanotubes: the competition of two-center and three-center bonding in boron sheets. *Phys. Rev. Lett.* **2007**, *99*, 115501, DOI: 10.1103/PhysRevLett.99.115501.

[9] Wu, X.; Dai, J.; Zhao, Y.; Zhuo, Z.; Yang, J.; Zeng, X. C., Two-dimensional boron monolayer sheets. *ACS nano* **2012**, *6*, 7443-7453, DOI: 10.1021/nn302696v.

[10] Penev, E. S.; Bhowmick, S.; Sadrzadeh, A.; Yakobson, B. I., Polymorphism of two-dimensional boron. *Nano Lett.* **2012**, *12*, 2441-2445, DOI: 10.1021/nl3004754.

[11] Zhou, X. -F.; Dong, X.; Oganov, A. R.; Zhu, Q.; Tian, Y.; Wang, H. -T., Semimetallic two-dimensional boron allotrope with massless dirac fermions. *Phys. Rev. Lett.* **2014**, *112*, 085502, DOI: 10.1103/PhysRevLett.112.085502.

[12] Li, W. -L.; Chen, Q.; Tian, W. -J.; Bai, H.; Zhao, Y. -F.; Hu, H. -S.; Li, J.; Zhai, H. -J.; Li, S. -D.; Wang, L. -S., The B35 cluster with a double-hexagonal vacancy: a new and more flexible structural motif for borophene. *J. Am. Chem. Soc.* **2014**, *136*, 12257-12260, DOI: 10.1021/ja507235s.

[13] Piazza, Z. A.; Hu, H. -S.; Li, W. -L.; Zhao, Y. -F.; Li, J.; Wang, L. -S., Planar hexagonal B36 as a potential basis for extended single-atom layer boron sheets. *Nat. Commun.* **2014**, *5*, 1-6, DOI: 10.1038/ncomms4113.

[14] Li, J.; Lv, H.; Lu, W.; Shao, D.; Xiao, R.; Sun, Y., Tuning the electronic and magnetic properties of borophene by 3d transition-metal atom adsorption. *Phys. Lett. A* **2016**, *380*, 3928-3931, DOI: 10.1016/j.physleta.2016.09.052.

[15] Meng, F.; Chen, X.; Sun, S.; He, J., Electronic and magnetic properties of pristine and hydrogenated borophene nanoribbons. *Physica E Low Dimens. Syst. Nanostruct.* **2017**, *91*, 106-112, DOI: 10.1016/j.physe.2017.04.014.

[16] Peng, B.; Zhang, H.; Shao, H.; Xu, Y.; Zhang, R.; Zhu, H., The electronic, optical, and thermodynamic properties of borophene from first-principles calculations. *J. Mater. Chem. C* **2016**, *4*, 3592-3598, DOI: 10.1039/C6TC00115G.

[17] Sun, H.; Li, Q.; Wan, X., First-principles study of thermal properties of borophene. *Phys. Chem. Chem. Phys.* **2016**, *18, 14927-14932, DOI: DOI:* 10.1039/c6cp02029a.

[18] Rastgou, A.; Soleymanabadi, H.; Bodaghi, A., DNA sequencing by borophene nanosheet via an electronic response: a theoretical study. *Microelectron. Eng.* **2017**, *169*, 9-15, DOI: 10.1016/j.mee.2016.11.012.

[19] Wang, J.; Du, Y.; Sun, L., Ca-decorated novel boron sheet: A potential hydrogen storage medium. *Int. J. Hydrogen Energ.* **2016**, *41*, 5276-5283, DOI: 10.1016/j.ijhydene.2016.01.039.

[20] Valadbeigi, Y.; Farrokhpour, H.; Tabrizchi, M., Adsorption of small gas molecules on B36 nanocluster. *Int. J. Chem. Sci.* **2015**, *127*, 2029-2038, DOI: 10.1007/s12039-015-0967-y.

[21] Kootenaei, A. S.; Ansari, G., B36 borophene as an electronic sensor for formaldehyde: quantum chemical analysis. *Phys. Lett. A* **2016**, *380*, 2664-2668, DOI: 10.1016/j.physleta.2016.06.016.

[22] Rostami, Z.; Soleymanabadi, H., N-H bond cleavage of ammonia on graphene-like B 36 borophene: DFT studies. *J. Mol. Model* **2016**, *22*, 70, DOI: 10.1007/s00894-016-2954-8.

[23] Omidvar, A., Borophene: A novel boron sheet with a hexagonal vacancy offering high sensitivity for hydrogen cyanide detection. *Comput. Theor. Chem.* **2017**, *1115*, 179-184, DOI: 10.1016/j.comptc.2017.06.018.

[24] Xu, S.; Dong, R.; Lv, C.; Wang, C.; Cui, Y., Configurations and characteristics of boron and B36 clusters. *J. Mol. Model* **2017**, *23*, 198. DOI: 10.1007/s00894-017-3377-x.

[25] Frisch, M.; Trucks, G.; Schlegel, H.; Scuseria, G.; Robb, M.; Cheeseman, J.; Scalmani, G.; Barone, V.; Mennucci, B.; Petersson, G., Gaussian 09, Revision A. 02, Gaussian, Inc., Wallingford, CT, 2009.

[26] Grimme, S., Semiempirical GGA-type Density functional constructed with a long-range dispersion correction. *J. Comput. Chem.* **2006**, *27*, 1787-1799, DOI: 10.1002/jcc.20495.

[27] Shakerzadeh, E., Quantum chemical assessment of the adsorption behavior of fluorouracil as an anticancer drug on the B36 nanosheet. *J. Mol. Liq.* **2017**, *240*, 682-693, DOI: 10.1016/j.molliq.2017.05.128.

[28] Lu, T.; Chen, F., Multiwfn: A multifunctional wavefunction analyzer. *J. Comput. Chem.* **2012**, *33*, 580-592, DOI: 10.1002/jcc.22885.

[29] Mayer, I.; Salvador, P., Overlap populations, bond orders and valences for 'fuzzy'atoms. *Chem. Phys. Lett.* **2004**, *383*, 368-375, DOI: 10.1016/j.cplett.2003.11.048.

[30] Lu, T.; CHEN, F.-W., Meaning and functional form of the electron localization function. *Acta Phys. Chim. Sin* **2011**, *27*, 2786-2792, DOI: 10.3866/PKU.WHXB20112786.

[31] Allal, H.; Belhocine, Y.; Rahali, S.; Damous, M.; Ammouchi, N., Structural, electronic, and energetic investigations of acrolein adsorption on B36 borophene nanosheet: a dispersion-corrected DFT insight. *J. Mol. Model* **2020**, *26*, 1-12, DOI: 10.1007/s00894-020-04388-3.

[32] Marana, N. L.; Casassa, S.; Longo, E.; Sambrano, J. R., Structural, electronic, vibrational, and topological analysis of single-walled zinc oxide nanotubes. *J. Phys. Chem. C* **2016**, *120*, 6814-6823, DOI: 10.1021/acs.jpcc.5b11905.

[33] Wu, Q. -Y.; Lan, J. -H.; Wang, C. -Z.; Zhao, Y. -L.; Chai, Z. -F.; Shi, W. -Q., Terminal U-E (E = N, P, As, Sb and Bi) bonds in uranium complexes: A theoretical perspective. *J. Phys. Chem. A* **2015**, *119*, 922-930, DOI: 10.1021/jp512950j.

[34] Chakraborty, D.; Chattaraj, P. K., In quest of a superhalogen supported covalent bond involving a noble gas atom. *J. Phys. Chem. A* **2015**, *119*, 3064-3074, DOI: 10.1021/jp513018v.